Published in final edited form as:
Cell. 2009 May 1; 137(3): 445–458. doi:10.1016/j.cell.2009.02.043.

Mechanisms that specify promoter nucleosome location and identity

Paul D. Hartley[1] and **Hiten D. Madhani**[1,2]

1*Department of Biochemistry and Biophysics, University of California, San Francisco, 600 16th St. MC2200, San Francisco, CA 94158*

SUMMARY

The chromatin architecture of eukaryotic gene promoters is generally characterized by a nucleosome-free region (NFR) flanked by at least one H2A.Z variant nucleosome. Computational predictions of nucleosome positions based on thermodynamic properties of DNA-histone interactions have met with limited success. Here we show that the action of the essential RSC remodeling complex in *S. cerevisiae* helps explain the discrepancy between theory and experiment. In RSC-depleted cells, NFRs shrink such that the average positions of flanking nucleosomes move toward predicted sites. Nucleosome positioning at distinct subsets of promoters additionally requires the essential Myb family proteins Abf1 and Reb1, whose binding sites are enriched in NFRs. In contrast, H2A.Z deposition is dispensable for nucleosome positioning. By regulating H2A.Z deposition using a steroid-inducible protein splicing strategy, we show that NFR establishment is necessary for H2A.Z deposition. These studies suggest an ordered pathway for the assembly of promoter chromatin architecture.

INTRODUCTION

Since the identification of a nucleosome-free region (NFR) in SV40 minichromosomes nearly 30 years ago (Jakobovits et al., 1980; Saragosti et al., 1980), the mechanisms underlying the positioning of nucleosomes have been an area of active study. Recent genome-scale surveys of nucleosome positions in a variety of eukaryotic organisms have revealed a stereotypical promoter chromatin architecture characterized by a nucleosome-free region (NFR) flanked by at least one nucleosome enriched for the histone H2A variant H2A.Z (Albert et al., 2007; Lee et al., 2007; Mavrich et al., 2008a; Mavrich et al., 2008b; Ozsolak et al., 2007; Raisner et al., 2005; Yuan et al., 2005). As a class, NFR-adjacent nucleosomes are the most precisely positioned in the genome, with neighboring nucleosomes displaying less precision in their locations as their distance from NFRs increases. By acting as anchor points, the tight positioning of NFR-flanking nucleosomes may be a dominant mechanism by which nucleosomes are positioned genome-wide (Mavrich et al., 2008a). In *S. cerevisiae*, NFR-flanking nucleosomes often occlude the transcription start site (TSS) such that the TSS is on average half a helical turn inside the +1 nucleosome and exhibits a rotational phasing which tends to place sites for transcription factors on the accessible surface of nucleosomal DNA (Albert et al., 2007). Significantly, recent detailed analysis of the *PHO* regulon in *S. cerevisiae* has shown that chromatin remodeling during phosphate starvation exposes a class

2Corresponding author: E-mail: hitenmadhani@gmail.com, tel 415-514-0594, fax 415-502-4315.

of binding sites for the Pho4 activator that are initially masked by nucleosomes and that this plays a key role in shaping the input-output functions of promoters (Lam et al., 2008). Defects in the positioning of some promoter nucleosomes seen in *isw2* mutant cells correlates with the accumulation of cryptic antisense transcripts, leading to the proposal that positioning of nucleosomes also prevents erroneous transcription initiation events (Whitehouse et al., 2007). While the fractional occupancy of H2A.Z in NFR-flanking nucleosomes in yeast is not correlated with transcription rates (Raisner et al., 2005), loss of promoter nucleosomes including those containing H2A.Z occurs in response to transcriptional activation (Bernstein et al., 2004; Schones et al., 2008; Shivaswamy et al., 2008; Zanton and Pugh, 2006). It has been reported that H2A.Z nucleosomes are less stable in vitro, and this property has been hypothesized to aid in their removal in vivo (Zhang et al., 2005). In *Drosophila* and humans, NFRs flanked by nucleosomes enriched in H2A.Z are also a common feature of promoters (Barski et al., 2007; Mavrich et al., 2008b). In flies, the H2A.Z nucleosomes at promoters tend to occur downstream of the NFR, whereas in humans there appear to be H2A.Z nucleosomes both upstream and downstream of NFRs. Interestingly, both NFR formation and H2A.Z deposition seem to correlate with productive transcription in these organisms. These species-specific differences suggest additional complexity in metazoans. H2A.Z nucleosomes are also relatively enriched at flanking non-promoter NFRs that characterize enhancers and insulators in human T-cells (Barski et al., 2007). Taken together, nucleosome-free regions, whether or not associated with gene promoters, tend to be associated with H2A.Z. A conserved function of H2A.Z demonstrated in both S. cerevisiae and Arabidopsis thaliana is to act in euchromatin to antagonize gene silencing (Meneghini et al., 2003; Zilberman et al., 2008).

Despite the high conservation across eukaryotic evolution of these basic aspects of promoter chromatin architecture identified by descriptive genomic studies, the mechanisms by which NFRs flanked by H2A.Z nucleosomes form remain poorly understood. There exists evidence that octamer positioning genome-wide is mediated by a genomic nucleosome positioning code in which intrinsic DNA-octamer affinities, predicted computationally based on dinucleotide periodicity patterns and/or other sequence patterns, are a significant determinant of location, particularly at NFR-flanking nucleosomes (Ioshikhes et al., 2006; Lee et al., 2007; Segal et al., 2006). For example, one study (Segal et al., 2006) reported that 50% of nucleosome positions in *S. cerevisiae* chromosome III can be accurately predicted computationally. However, there are differences of opinion in the literature regarding how well computational methods predict actual positions determined experimentally compared to so-called random guess predictions (Peckham et al., 2007; Segal, 2008; Yuan and Liu, 2008). A recent study (Yuan and Liu, 2008) compared a number of methods and found that for *S. cerevisiae* datasets even improved methods required an error of ~70bp (nearly half a nucleosome) to obtain a prediction sensitivity of 80% and required a similar error to yield an specificity of 80%. These errors stand in contrast to the observed precision of nucleosome positioning in vivo relative to TSSs and transcription factor binding sites as described above.

The connection between NFR formation and H2A.Z deposition is likewise not well-defined. One report suggested that H2A.Z deposition plays a role in nucleosome positioning, while another proposed that H2A.Z deposition has no role (Guillemette et al., 2005; Li et al., 2005). H2A.Z nucleosomes have been reported to be poor in vitro substrates of chromatin remodeling enzymes compared to their H2A counterparts (Li et al., 2005). Thus, whether NFR formation is required for H2A.Z deposition or vice versa is unknown.

In the absence of a consensus view of how promoter chromatin architecture is specified with precision, we sought to clarify the underlying mechanisms. In previous work, we identified a segment of the *SNT1* promoter required for normal levels of H2A.Z deposition. Remarkably, insertion of a short segment of this region into the middle of a transcriptionally quiescent *PRM1* gene resulted in the formation of an NFR flanked by two nucleosomes containing H2A.Z

(Raisner et al., 2005). This sequence contained a putative binding site for the Myb family transcription factor Reb1 and an adjacent T tract. Below we describe further studies of this synthetic NFR as well as chromosome-wide studies of the roles of several essential factors in nucleosome positioning and H2A.Z deposition.

RESULTS

Models for NFR formation and H2A.Z deposition

We considered three models by which the DNA signal containing the Reb1 binding motif (henceforth called Reb1:dT_7) might program promoter chromatin structure (Fig. 1A, Fig. 1B). In Model I, the DNA signal first programs NFR formation, and then the NFR acts as a signal to induce H2A.Z deposition into the flanking nucleosomes. Model II proposes the reverse process of NFR formation such that a DNA signal first induces H2A.Z deposition, and H2A.Z then acts as a signal for NFR formation. Lastly, NFR formation and H2A.Z deposition could occur in an independent, uncoupled fashion (Model III). To distinguish these models, we first sought to define *trans*-acting factors that mediate NFR formation.

Construction of conditional degron alleles of Reb1, Abf1 and the RSC ATPase Sth1

The mechanism by which Reb1:dT_7 induces formation of an NFR flanked by two nucleosomes carrying H2A.Z likely involves the recruitment of Reb1, although this was not tested directly in our previous study. We also hypothesized that Reb1 might recruit a chromatin remodeling enzyme to produce an NFR. A systematic study of protein interactions revealed that Reb1 physically associates with Rsc2, Rsc3 and Npl6, which are subunits of the essential chromatin remodeling complex RSC (Cairns et al., 1996; Cairns et al., 1999; Gavin et al., 2002). Since the Reb1-related factor, Abf1, has also been implicated in the formation of a nuclease-sensitive site (De Winde et al., 1993), we pursued its functional role.

As Reb1, Abf1, and the catalytic subunit of RSC (Sth1) are all essential proteins, we generated a series of conditional alleles Specifically, we used the temperature-sensitive degron system to engineer yeast strains in which we could control degradation of these proteins via the N-end rule pathway (Dohmen and Varshavsky, 2005). This pathway operates through the recognition of destabilizing N-terminal amino acids by the nonessential E3 ubiquitin ligase Ubr1. A N-terminal arginine is the strongest signal for degradation by Ubr1, and traditional degron alleles encode proteins capped by an arginine followed by a temperature-sensitive murine dihydrofolate reductase ($DHFR^{ts}$) peptide fused to the target protein. As translation initiates at an ATG codon, an ATG-initiated segment encoding a ubiquitin moiety is placed before the arginine codon. Once synthesized, this segment is cleaved in cells by ubiquitin C-terminal proteases to expose the N-terminal arginine. Such degron systems also place the modified allele of interest under the control of a regulatable promoter, which traditionally has been the copper-inducible promoter *pCUP1*.

We constructed *pCUP1::UBI4::DHFR^{ts}::c-myc::STH1* and *pCUP1::UBI4::DHFR^{ts}::c-myc::REB1* alleles in strains that had *UBR1* under the control of the *pGAL1* promoter. We were unable to achieve substantial degradation of these proteins or growth arrest under degron-inducing conditions, although such an allele for *STH1* has been reported (Parnell et al., 2008). We achieved more complete degradation of Reb1 and Sth1 under degron-inducing conditions with a different construct (*pMET3::UBI4::DHFR^{ts}::3xHA*) that utilized the methionine-repressed *pMET3* promoter (Fig. 1C). Yeast strains carrying Reb1-degron or Sth1-degron alleles were inviable under degron-inducing conditions (Fig. 1D). While an Abf1 $DHFR^{ts}$ degron has been reported in the W303 strain background (Reed et al., 1999), we were unable to construct a viable *pMET3::UBI4::DHFR^{ts}::3xHA::ABF1* degron allele in our S288C background despite several attempts and strategies. We, however, successfully created a

pMET3::UBI4::abf1(M1R) allele in a strain carrying a *pGAL1::UBR1* allele. As described above, the ubiquitin moiety of the translated protein is cleaved off soon after translation, leaving an Abf1 protein capped with a destabilizing N-terminal arginine. Under inducing conditions, this Abf1-degron yielded growth arrest and displayed Abf1 depletion (Fig. 1C, 1D). We also constructed an Abf1 Reb1 "double degron" strain in order to simultaneously deplete both factors from cells (Fig. 1C, 1D). For the studies described below, we determined nucleosome positions by hybridizing mononucleosomal versus genomic DNA-derived probe with in-house printed custom tiling arrays that span *S.cerevisiae* chromosome III at 20bp resolution (Yuan et al., 2005). The arrays also included oligonucleotides that tiled sequences corresponding to the *PRM1* gene to allow us to observe nucleosome positions programmed by Reb1:dT_7 (see Experimental Procedures for details). Unless otherwise specified, all experiments represent averages of four independent, biological replicates.

NFR formation mediated by a Reb1 binding site requires Reb1 and the chromatin remodeling complex RSC, but not H2A.Z

As expected from our previous study (Raisner, et al., 2005), nucleosome position analysis of the *PRM1* ORF with or without a Reb1:dT_7 insertion revealed that the insertion produces an NFR (Fig. 2A). NFR formation was unaffected in strains carrying the Reb1-degron or Sth1-degron alleles under conditions in which the degron system was inactive (Fig. 2B). We mapped nucleosome positions in strains carrying the Reb1-degron or the Sth1-degron five hours after activating the degron system, and these positions were compared to nucleosome positioning data from a control strain isogenic to the degron strains except that it lacked the Reb1 or Sth1 degron allele. The latter control strains were subjected to the identical culture growth protocol as the experimental strains. Depletion of Reb1 resulted in loss of the NFR programmed by Reb1:dT_7 inserted into the *PRM1* ORF, consistent with a direct role for Reb1 (Fig. 2B). Likewise, inactivation of the RSC complex through depletion of Sth1 resulted in complete loss of the NFR programmed by the Reb1:dT_7 sequence (Fig. 2B), supporting the hypothesis that Reb1 functions by recruiting RSC.

Model II above proposes that NFR formation requires the prior deposition of H2A.Z into chromatin, which is mediated by the Swr1 chromatin remodeling complex. We tested whether H2A.Z or Swr1 is required for NFR formation induced by the Reb1:dT_7 signal. We constructed *htz1Δ* and *swr1Δ* strains and mapped the nucleosome positions in these strains. NFR formation meditated by insertion of Reb1:dT_7 at *PRM1* did not require H2A.Z or Swr1 (Fig. 2C).

To test whether NFR formation at *PRM1* might be a consequence of transcription, we examined whether NFR formation induced by Reb1:dT_7 was associated with the production of transcripts. Transcript levels were examined using RT-PCR analysis of extracted total RNA. In a control strain in which the *PRM1* gene was induced with mating pheromone for 1hr, a specific signal was obtained (Fig. S10A). We examined strains containing the insert and the Sth1 degron under both degron-inducing and permissive conditions as well as a strain lacking the insert. In these three cases, multiple peaks rather than a single peak were obtained in the QPCR melting curves indicating that cross-reacting cDNAs, instead of products specific to the *PRM1* locus, were being detected. Moreover, no quantitative differences were observed (Fig. S10A). Taken together, these data suggest that NFR formation was not associated with transcription that could be detected by these methods.

Reb1 is required for the formation of a subset of NFRs

We next examined the chromosome-wide requirement for Reb1 in NFR formation. We mapped and compared nucleosome positions in the Reb1-degron strain and an isogenic control strain that lacked the Reb1-degron under conditions described above. Fig. 3A shows a gene-by-gene "difference map" of the positioning data in which genes were aligned to each other based on

the position +1 nucleosome downstream of the NFR in control strains and then the mutant signal subtracted from the control signal (yellow indicates more nucleosomal DNA signal in the mutant than in wild-type cells). The data were organized by K-means clustering. Two clusters are evident, one in which positioning was affected (Cluster I affecting 12% of assayed promoters), and another where no effect was evident (Cluster II). Line traces of the average signals of the control and degron strains for these two clusters are shown in Fig. 3B. Inspection of Cluster I indicates that the two NFR-flanking nucleosomes move inward towards the center of the NFR, and this movement propagates further such that other flanking nucleosomes also shift their positions (Fig 3B) Figure 3C shows that the changes in the size of the trough signal representing the NFR between degron and control strains were dependent on the induction of the degron.

A previous study of transcription factor association at promoters assigned likelihood scores for a given transcription factor binding to a given promoter (Harbison et al., 2004). We compared these scores for Reb1 to the highest fold-change probe in the NFRs of promoters we assayed that were assigned scores. As shown in Fig. 3D, there was a significant correlation ($p=7.81\times10^{-7}$ based on a hypergeometric test using a likelihood score cutoff of $p<0.05$). Consistent with this finding, promoters that contained at least one copy of the most conserved Reb1 binding site (TTACCCG, (Liaw and Brandl, 1994)) tended to experience changes in NFR structure (Fig. 3E). Cluster I was enriched for the most conserved Reb1 consensus site; indeed, 14 out of the 18 promoters in Cluster I contained this motif ($p= 5.07\times10^{-13}$, Fig. 3F). Relaxing the consensus to reflect the poorer conservation of the first two residues of the consensus still yielded highly significant enrichments (Fig. 3F).

Abf1 is required for the formation of a subset of NFRs

We next performed the same analysis on Abf1 degron strain. Difference map analysis and clustering (Fig. 4A) show that 9.3% of promoters were affected, and these promoters were distinct from promoters affected by Reb1 depletion (see below). As with the Reb1 degron, the affected cluster displays a smaller NFR and movement of flanking nucleosomes towards the NFR (Fig. 4B), and these changes were dependent on induction of the degron (Fig. 4C). Likewise, affected NFRs were enriched for Abf1 binding (Fig. 4D) and for an Abf1 consensus site (Fig. 4E, F). The latter correlations are weaker than for the Reb1 site, perhaps because of the higher degeneracy of the Abf1 consensus site (Beinoraviciute-Kellner et al., 2005).

RSC is required for proper positioning of NFR-flanking nuclesomes

We next examined the effects of Sth1 depletion on nucleosome positioning using strains carrying the Sth1-degron as described above. Strikingly, our analysis showed that Sth1 depletion affected a majority (55%) of promoters (see Cluster I in Fig. 5A). The affected cluster displayed shrinking of the NFR and movement of flanking nucleosomes, whereas little change in nucleosome position was apparent for members of Cluster II (Fig. 5B). As with the Reb1 and Abf1 degron strains, growth under degron-inducing conditions was required to observe these differences (Fig. 5C). Fig. S10B shows a superposition of a histogram of the locations of mapped TSSs (Nagalakshmi, et al., 2008) and the positioning data. Consistent with previous studies, TSSs tend to lie just inside the downstream nucleosome and the movement observed in Sth1-depeleted cells moves these sites further into the nucleosome core (Fig. S10B). This may explain why RSC depletion has been reported to cause cessation of transcription by RNA polymerase II (Parnell et al., 2008).

When RSC, Abf1, or Reb1 were depleted, NFRs shrank but were not eliminated. We hypothesized that intrinsic positioning sequences might explain the positions of nucleosomes under these conditions. Therefore, we compared the positions we observed in Cluster I of Sth1-depleted cells with those predicted by Pugh and colleagues (Ioshikhes et al., 2006) based on

AA/TT dinucleotide periodicity enrichment. As shown in Figure 5E, the average nucleosome position of the +1 and -1 nuclesomes of Cluster I relax towards positions specified by the NPS signature. For the largely unaffected cluster (Cluster II), a discrepancy between the NPS-predicted and observed positions is still apparent for the +1 nucleosome, whereas the -1 nucleosome is poorly aligned in this despite the sharp NPS prediction peak (Fig. 5E).

To test whether Sth1 depletion results in changes in gene expression, we performed expression profiling of the Sth1 degron strain against a control strain under degron-inducing conditions. As we expected global changes in gene expression, we incorporated external spiked-in RNA controls into our normalization procedure (see Experimental Procedures). We then asked whether there was an enrichment for genes whose expression was reduced in Sth1-depleted cells in Cluster I vs. Cluster II. As shown in Figure 5D, Cluster I is indeed highly enriched for genes whose expression requires Sth1, indicating that that the changes in positioning correlate with changes in expression. Given this result, we tested whether loss of transcription might be responsible for changes in positioning. We mapped nucleosome positions in a temperature-sensitive RNA polymerase II strain (*rpb1-1*) which ceases transcription within minutes upon shift into restrictive conditions (Nonet et al., 1987). The *rpb1-1* mutant was grown at either 25°C or shifted for 1 hour to 37°C. The average nucleosome positions in these conditions were determined for Clusters I and II of the Sth1 degron difference map. There were were no detectable differences in nucleosome positions in either cluster (Fig. 5F, Fig. S10C). Hence, the changes in NFR structure observed upon Sth1 depletion appear to be due to the action of RSC rather than from cessation of transcription *per se*.

Abf1 and Reb1 are required for NFR formation at distinct sets of promoters

To identify promoters that are redundantly controlled by Abf1 and Reb1, we examined a double degron strain that carried the Abf1-degron and Reb1-degron alleles (Fig.1C, 1D). The resulting difference map was clustered together with difference maps for the Abf1 single degron strain, the Reb1 single degron strain, and the Sth1 degron strain (Fig. 6A; Fig. 6B shows that NFR changes in the double degron are dependent on degron induction). K-means clustering revealed that the promoter NFRs affected by loss of either Abf1 or Reb1 were reproducibly affected in the double degron strain, but there were no other promoter NFRs that were significantly affected in the double degron strain. It is also evident that most NFRs affected by loss of Reb1 also required Sth1 for proper positioning of nucleosomes (Fig. 6A), consistent with the data obtained with the synthetic NFR described above (Fig. 2B). The NFRs affected by loss of Abf1 appeared to have a somewhat lesser degree of dependence for Sth1 for nucleosome positioning (Fig. 6A). Likewise, there clearly are many NFRs that require RSC, but not Abf1 or Reb1, for proper nucleosome positioning (Fig. 6A), suggesting the existence of additional RSC recruitment mechanisms. Analysis of average nucleosome positions for each cluster indicates that the the changes observed (Fig 6A) are due to shifts in nucleosome positions (Fig. S14).

As with the Sth1 degron strain, we examined the Abf1-Reb1-double-degron strain for changes in transcript levels using whole genome microarrays and spiked-in external controls. As shown in Figure 6C, we found a significant correlation between decreases in NFR size and decreases in transcript accumulation.

H2A.Z deposition is generally dispensable for nucleosome positioning

To complete our analysis of positioning, we used cells lacking H2A.Z (*htz1*Δ) or lacking the ATPase subunit of its deposition complex (*swr1*Δ) to determine whether H2A.Z exchange was required for nucleosome positioning chromosome-wide (Fig. 7). Based on the results with the synthetic NFR (Fig. 2C), we expected to see no differences in positioning. Indeed, as shown by line traces of the average positions of aligned promoter nucleosomes, H2A.Z deposition

resulted in no detectable changes. Of course, we cannot rule out the possibility that there could be changes too subtle to observe using our 20bp resolution tiling arrays.

Development an inducible H2A.Z deposition system

Nonetheless, these data argue against Model II (Fig. 1B), which proposed that H2A.Z deposition is essential for NFR formation. We then considered the two remaining models: (1) the deposition of H2A.Z at a promoter requires the presence of an NFR at that promoter (Model II), or (2) H2A.Z deposition occurs independently of NFR formation (Model III). In principle, these models could be distinguished through development of a system in which NFR loss is induced under conditions where H2A.Z is not deposited into chromatin, but then H2A.Z is induced and its deposition examined. The Sth1 degron provides a tool to trigger abrogation of the synthetic NFR programmed by Reb1:dT_7 and a shrinkage of bona fide promoter NFRs. However, since global transcription is shut off in RSC-depleted cells, we sought a posttranslational method to control H2A.Z deposition.

We utilized an engineered *M. tuberculosis* RecA intein whose intrinsic protein splicing is controlled by the human estrogen receptor ligand binding domain (Buskirk et al., 2004). This construct was used previously to interrupt several coding sequences in yeast, and its splicing was shown to be activated in vivo using the estrogen agonist 4-hydroxytamoxifen (4-HT). The chemistry of splicing requires cysteine cleavage sites and leaves a single cysteine residue at the splice junction.

We initially targeted the Swr1 and Swc2 subunits of the Swr1 complex by inserting the intein construct before the codons for several native cysteine residues in the corresponding genes. These alleles abrogated H2A.Z deposition in *vivo*, but addition of 4-HT did not restore H2A.Z deposition (unpublished observations), suggesting that the placement of the intein was incompatible with protein stability and/or intein splicing. We next attempted engineering a spliceable *HTZ1* allele under the assumption that the smaller size of H2A.Z relative to the intein construct would make the protein context less likely to interfere in proper structural formation of the intein. H2A.Z, however, lacks cysteine residues, so such a spliced allele would by necessity contain a cysteine point mutation. Four H2A.Z residues (Ala46, Thr68, Thr88 and Asp100) that did not confer a significant growth defect in high precision measurements when mutated (S. Braun, D. Breslow, J. Weissman, H. D. M., unpublished observations) were replaced with the intein construct. These alleles initially replaced wild-type *HTZ1* at its native chromosomal locus, but none displayed detectable spliced product in the presence of 4-HT (unpublished observations). We therefore placed these alleles under the control of a *pGAL1* promoter on a high-copy 2 micron plasmid vector. The allele in which Ala46 was replaced with the intein construct yielded a protein that was spliced in vivo when cultures were treated with 4-HT; Ala46 is a residue in the core histone fold domain (Fig. 8A, 8B). As splicing produced somewhat higher levels of H2A.Z than in that found in wild-type cells (Fig. 8B), we placed the construct on a low-copy *CEN-ARS* plasmid. Regulated splicing of the H2A.Z intein was also observed (Fig. S13A), and this construct was used in further experiments. We refer to this *pGAL1::htz1(A46intein)* allele on a *CEN-ARS* plasmid as the H2A.Z intein construct.

We examined the deposition of H2A.Z whose synthesis was directed by this construct using chromatin immunoprecipitation (ChIP). Although splicing in the H2A.Z intein is regulated, a small amount of H2A.Z deposition was observed in the absence of 4-HT, presumably due to low levels of background splicing (Fig. S13C); however, the H2A.Z enrichment signal steadily increases over time in response to 4-HT treatment (Fig S13D), indicating stimulation of H2A.Z deposition by the activation of splicing.

Focused H2A.Z deposition in response to Reb1:dT$_7$ requires prior NFR formation by RSC

We introduced the H2A.Z intein into *htz1Δ* strains that carried *pGAL1::UBR1* and either the Sth1-degron or a wild-type Sth1. Simultaneous activation of the degron system and synthesis of unspliced H2A.Z were accomplished by transferring cells to 37°C media containing galactose. After 5 hours of growth, intein splicing was initiated by the addition of 4-HT, and cells were collected after 3 hours of further incubation at 37°C to allow for H2A.Z deposition. Chromatin immunoprecipitation for H2A.Z and histone H3 were carried out, and quantitative PCR was used to measure H2A.Z enrichment relative to H3 enrichment. The H2A.Z/H3 enrichment values were normalized to an amplicon in the middle of the large *BUD3* ORF where there is little detectable H2A.Z (Raisner et al., 2005). Nucleosome positions were also mapped for the Sth1-degron H2A.Z intein strain prior to degradation of Sth1, after 5 hours of Sth1 depletion, and 3 hours after addition of 4-HT. We determined that unspliced H2A.Z was being produced and was spliceable, and we found that Sth1 degradation still occurred in the presence of the H2A.Z intein construct and during 4-HT treatment (Fig S13A, B).

We sought to examine the deposition profiles of H2A.Z at NFRs whose structure is unaffected upon Sth1 depletion and at NFRs that undergo significant changes upon Sth1 depletion. The two NFRs located within an intergenic region containing the *DCC1* and *BUD3* promoters do not appear to require Sth1 for their organization (Fig. 8C, top panel). The H2A.Z deposition profiles across the *DCC1-BUD3* intergenic region in both the Sth1-degron and control strains were similar (Fig. 8C bottom) and indicated that H2A.Z deposition could still occur under these conditions. We next examined how loss of the NFR programmed by insertion of Reb1:dT$_7$ into *PRM1* affected the recruitment of H2A.Z. This NFR essentially collapses upon Sth1 depletion in the H2A.Z intein strain carrying the Sth1-degron (Fig. 8D, top panel). In the strain that did not have the Sth1-degron and therefore maintained the NFR programmed by Reb1: dT$_7$ inserted into *PRM1*, H2A.Z deposition occurred in the middle of *PRM1*, with its peak deposition at the Reb1: dT$_7$ insertion site (Fig. 8D, bottom left panel). In contrast, upon Sth1 depletion, there was no H2A.Z deposition focus about the Reb1: dT$_7$ insertion site (Fig. 8D, bottom right panel). The apparently undirected, background H2A.Z deposition in the *PRM1* ORF is similar to that observed in cells lacking the Reb1:dT$_7$ insertion (Raisner et al., 2005), and similar global patterns of untargeted H2A.Z deposition have been seen in genome-wide studies (Albert et al., 2007). Thus, the focused peak of H2A.Z deposition induced by the Reb1:dT$_7$ DNA signal appears to require the Sth1-dependent formation of an NFR directed by the signal.

RSC depletion did not produce complete collapse of NFRs on endogenous promoters, and, as described above, this may be due to intrinsic positioning signals. Nonetheless, we examined the H2A.Z deposition profile at the promoters of *YCR016W* and *YCR023C*, both of which experience significant nucleosome encroachment into their NFRs upon Sth1 depletion (Fig. 8E and 8F, top panels). We observed H2A.Z deposition at these promoters under conditions in which their NFRs were unaffected as well as under conditions where their NFRs were affected (Fig. 8E and 8F, bottom panels). However, the H2A.Z deposition profile at affected NFRs differed in that there was a significant decrease in H2A.Z enrichment in the vicinity of the +1 nucleosome relative to the NFR (see amplicon “D” for Fig. 8E and amplicon “C” for Fig. 8F). Whether the otherwise fairly robust H2A.Z deposition seen at these two promoters under conditions of intein induction is explained by the presence of a residual NFR driven by NPSs or by NFR-independent mechanisms that stimulate H2A.Z deposition such as histone acetylation and its subsequent recognition by Bdf1 (Raisner et al., 2005) is not clear. The latter model is difficult to test since cells lacking H2A.Z and Bdf1 are inviable (Raisner et al., 2005).

DISCUSSION

Based on the results of a number of genome-scale studies, it has become increasingly clear in organisms as diverse as yeast and humans that gene regulatory regions display stereotypical patterns of nucleosome positioning and identity. Although there are species-specific differences, promoters are generally characterized by an NFR flanked by at least one H2A.Z nucleosome. Despite the power of these descriptive genome-wide studies as well as work that indicates that these characteristics of promoters play key roles in gene regulation (see Introduction for references), they leave open the question of how these structures are programmed.

Two lines of studies have come to distinct conclusions regarding NFR formation mechanisms. One group of studies has suggested that the direct effects of sequence on DNA-octamer affinity programs NFR formation (see Introduction for references). In contrast, our previous work defined a short signal from the *SNT1* gene containing a putative site for a DNA binding protein, Reb1, that is sufficient to program a NFR flanked by H2A.Z nucleosomes when placed into the middle of a positioned nucleosome in an inactive gene (Raisner et al., 2005). Others have also implicated Reb1 and Abf1 in the formation of nucleosome gaps within the specific promoter regions (Angermayr et al., 2003; De Winde et al., 1993). The work described here helps reconcile these two lines of research and provides insight into the relationship between NFRs and H2A.Z deposition. Our principal conclusions are as follows:

(1) RSC displaces NFR-flanking nucleosomes away from their average NPS-predicted positions

A striking result presented here is that at a majority of promoters, the normal positioning of NFR-flanking nucleosomes requires the essential multisubunit chromatin modeling complex RSC. Such a central role for RSC in generating promoter chromatin architecture is consistent with several of its properties: 1) RSC, unlike most chromatin remodeling enzymes in yeast, is essential for viability (Cairns et al., 1996; Cairns et al., 1999), 2) RSC slides nucleosomes in vitro (Lorch et al., 2001), and 3) RSC is required globally for RNA polymerase II transcription (Parnell et al., 2008). Our studies are also consistent with a recent lower-resolution study that concluded that RSC affected histone density at a number of promoters (Parnell et al., 2008). A recent study indicated changes in the positioning nucleosomes at ~12% of promoters in cells lacking the Isw2 chromatin remodeling complex (Whitehouse et al., 2007). The primary function of Isw2 appears to be in transcriptional repression and in suppressing antisense transcription (Whitehouse et al., 2007). Interestingly, in contrast to RSC, Isw2 appears to move nucleosomes in vivo toward the NFR, raising the possibility that it antagonizes the action of RSC at some promoters. The potential for dynamic involvement of multiple ATPases at promoters further underscores the active nature of mechanisms that position nucleosomes in vivo.

The finding in this study and in the previous study that the final resting positions of nucleosomes are strongly influenced by ATP-dependent chromatin remodeling mechanisms argues that that the intrinsic affinity of the octamer for underlying DNA sequences is not determinative for the final positioned state. However, our observation that depletion of Sth1 causes nucleosome positions to relax on average closer to those predicted by an NPS signature strongly suggests that sequence properties play a role in a stepwise mechanism for NFR formation. That is, NPS-mediated positioning exposes binding sites for factors such as Reb1 and Abf1, which in turn induce the action of RSC to move nucleosomes to their steady-state average positions in wild-type cells. Such a model is also consistent with in vitro and in vivo observations that suggest that the Isw2 remodeling enzyme moves nucleosomes into energetically unfavorable sites (Whitehouse and Tsukiyama, 2006). We speculate that, compared to a purely “hard-wired” system, this more dynamic, ATP-dependent mechanism may facilitate binding of DNA binding

proteins to nucleosomal sites and transcription initiation. It is important to note that NPS predictions vary in their accuracy considerably at the level of individual genes, suggesting they likely do not predict with full accuracy the intrinsic thermodynamics of octamer-DNA interactions. A histogram of predictions (Ioshikhes et al., 2006) reveals that NPS-predicted positions for individual genes deviate significantly from experimental positions even in the Sth1 degron strain (Fig S15). Nonetheless, the close correspondence of the average profiles supports the two-step model proposed above.

(2) Sequence-specific DNA binding proteins are required for positioning of NFR-flanking nucleosomes at a significant fraction of promoters

Using a signal for NFR formation/H2A.Z deposition we identified previously, we demonstrated a role for the Reb1 protein and RSC for NFR formation programmed by this isolated signal. Given the previously reported biochemical interactions between Reb1 and subunits of RSC, the simplest interpretation is that recruitment of RSC by Reb1 generates the NFR. Our examination of the generality of this mechanism across chromosome III suggests that a subset of promoters, enriched for Reb1 binding sites, use this mechanism in a nonredundant fashion. Abf1, another essential Myb family member, operates at a distinct subset of promoters. These observations are consistent with studies that show that Reb1 and Abf1 sites are highly enriched in NFRs compared to the binding sites for nearly all other studied DNA binding proteins (Lee et al., 2007). The remaining promoters presumably target RSC and other remodeling mechanisms through other means. In this regard, it is interesting to note that four subunits of RSC contain potential DNA binding domains. Using standard ChIP protocols as well as ones using additional crosslinking agents, we have been unable to detect either wild-type Sth1 or an induced catalytically-dead version of Sth1 at the Reb1:dT_7 signal inserted into *PRM1*, suggesting transient binding of RSC to this site (unpublished data). Likewise, only a fraction of intergenic regions display RSC binding in published ChIP-chip experiments (Ng et al., 2002), despite the global requirement for RSC in pol II transcription (Parnell et al., 2008). We suggest that at many sites of action the off-rate of the RSC complex in vivo may be too high to allow detection by ChIP.

(3) H2A.Z deposition is dispensable for NFR formation but NFR formation promotes H2A.Z deposition

We find no evidence that nucleosome positioning in general requires H2A.Z deposition. While a previous report suggested that H2A.Z controls nucleosome positioning *in vivo*, this conclusion was largely based on a single 20bp shift observed in the position of a nucleosome in the *GAL1* promoter in *htz1Δ* cells (Guillemette et al., 2005). Another study examined nucleosome positioning in *htz1Δ* cells at four other loci (*SUC2*, *COQ3*, *POS5*, and *COQ1*), which are all highly enriched for H2A.Z and saw no differences in positioning (Li et al., 2005). Our results are generally in line with the latter study. However, we note that the technology used in our study, while cost-effective and allowing for multiple experimental replicates, does not have the ability to detect shifts of less than 20bp. Thus, we cannot rule out the possibility that our studies would have missed a more subtle role for H2A.Z deposition in nucleosome positioning.

To explore the relationship between NFR formation and H2A.Z deposition we implemented a steroid-regulated protein splicing strategy to induce H2A.Z deposition under conditions in which NFR structure was abrogated by depletion of Sth1 Our data show that deposition of H2A.Z about the NFR programmed by insertion of Reb1:dT_7 into *PRM1* required the prior action of Sth1, which presumably acts to induce formation of the NFR. This defect in deposition was not due to a general defect in H2A.Z deposition in RSC-depleted cells as normal deposition occurred at the *BUD3-DCC1* intergenic region and significant albeit reduced H2A.Z deposition occurred at the promoters of two genes whose NFRs shrank in response to RSC depletion. Our

results predict that in vitro studies of the exchange activity of the purified Swr1 deposition complex may show a dependence on adjacent nonnucleosomal DNA. Such a property would not be without precedence as the ACF complex has been shown to have nucleosome-sliding catalytic activity that is stimulated in vitro by flanking DNA (Yang et al., 2006). These observations may explain the general linkage observed in yeast, plants and metazoans between NFRs of various sizes and enhanced deposition of H2A.Z in flanking nucleosomes.

EXPERIMENTAL PROCEDURES

Yeast strains

The strains used in this study are described in Table S1. Yeast transformants were generated by conventional lithium acetate and polyethylene glycerol procedures with selectable or counter-selectable transforming DNA. Insertions at the *PRM1* ORF were obtained by a two-step process in which a construct containing I-SceI and its restriction site was first inserted and subsequently replaced with a desired sequence (Storici, et al. 2003).

Antibodies

H2A.Z-specific polyclonal antisera were generated against a peptide specific for the C-terminus of *S. cerevisiae* H2A.Z (custom-generated). The HA epitope tag in the degron alleles was detected using monoclonal antibody HA.11 (Covance). Abf1 was detected using polyclonal antibodies directed towards the Abf1 C-terminus (yC-20, Santa Cruz). Histone H3-specific polyclonal antibodies were directed towards the C-terminus of human histone H3 (ab1791, abcam).

Microarray data

Microarray data can be obtained from NCBI GEO at series accession GSE13446.

Chromatin immunoprecipitation and QPCR

Chromatin immunoprecipitation and subsequent analysis by QPCR was performed as previously described (Raisner, et al., 2005, Meneghini, et al., 2003).

Gene expression profiling

For each strain, total RNA from four independently grown cultures was prepared using a TRIZOL procedure and spiked with RNA from the Agilent Dual-color RNA Spike-in Kit. Aminoallyl-dUTP-labeled probe was generated by reverse transcription, and hybridizations were carried out using 4×44k Agilent microarrays that cover 6256 *S. cerevisiae* features, each of which are replicated 7 times on the array (Agilent design ID 015072). Dye swaps were incorporated such that for each experiment, there were 2 arrays of one dye configuration, and vice-versa. Data normalization was performed using a composite loess procedure that used 1:1 DCP probes for the spike-in loess curve (Yang, et al. 2002). Expression ratios for each gene per array then were derived by calculating the mean of up to 7 technical replicates, while discarding any replicates that were not within 2 standard deviations.

Assaying the requirement of essential genes with degron technology

The essential genes *ABF1*, *REB1*, and *STH1* were studied by regulated degradation of their encoded protein via degron alleles. Each degron allele was under the control of the *pMET3* promoter, which is repressed by methionine. The *REB1* and *STH1* degron alleles had an arginine-capped N-terminal fusion of *DHFRts* and a triple-HA tag, while the *ABF1* degron allele was an *abf1(M1R)* allele. UBR1, the N-end rule pathway E3 ubiquitin ligase, was placed under the control of a *pGAL1* promoter.

To study phenotypes arising from loss of Abf1, Reb1 or Sth1, degron cultures were grown at 30°C to mid-log phase in synthetic complete media lacking methionine and cysteine with 2% raffinose and 0.1% dextrose as carbon sources. Activation of the degron was achieved by first adding galactose to a final concentration of 2% for 30 min, followed by centrifugation at room temperature to collect the cells. These cells were next grown at 37°C in rich media prewarmed at 37°C and supplemented with 2% galactose (YPAG).

Preparation of DNA for mapping nucleosome positions

Cultures in mid-log phase (which ranged from an OD_{600} of 0.7-0.9) were crosslinked with 1% formaldehyde for 15 min at the same temperature used for growth, followed by a quenching step for 5 min at room temperature with 0.125M glycine. Cells were washed twice with cold ddH_2O prior to storage.

Approximately 20 OD_{600} units of cells were spheroplasted with 0.25 mg Zymolyase 100-T (Seikagaku) in 2 ml Buffer Z (1M sorbitol, 50mM Tris-Cl pH 7.4, 10mM β-mercaptoethanol) at 30°C with shaking. The spheroplasting time ranged from 30 min to 75 min, depending on the strain and media conditions used for growth. The ideal spheroplasting time was one that yielded appropriately digested chromatin (~90% mononucleosomal-sized DNA) after 20 min of micrococcal nuclease (MNase) treatment. Spheroplasts were collected by centrifugation at 4°C and resuspended in 500μl MNase digestion buffer (0.075% NP-40, 50mM NaCl, 10mM Tris-Cl pH 7.4, 5mM $MgCl_2$, 1mM $CaCl_2$). Chromatin was digested with 3 units of MNase (Worthington) for 20 min at 37°C. Digestions were quenched with 50mM EDTA, and spheroplasts were lysed with 0.1% SDS and centrifuged to transfer the supernatant away from insoluble material. The supernatant containing solublized chromatin was incubated at 65°C overnight with 0.4 mg/ml proteinase K to deproteinize DNA and reverse methylene crosslinks. DNA was recovered by two extractions with phenol and one extraction with chloroform, followed by ethanol precipitation and resuspension in Tris-EDTA (TE) pH 8.0 supplemented with 10 μg/ml RNase A. After a 30 min treatment at 37°C, the DNA was ready for probe generation by linear amplification.

Preparation of reference genomic DNA

Genomic DNA was prepared by purification with a Qiagen 100 column after treating spheroplasts with RNase A and proteinase K. Purified DNA was digested with MNase at room temperature to obtain DNA that ranged in size from 100-300bp. This digested DNA was phenol-extracted twice, chloroform-extracted once, and then ethanol-precipitated and resuspended in TE pH 8.0. Genomic reference probe was then prepared by linear amplification in the same manner as mononucleosomal-sized probe.

Linear amplification of DNA to generate microarray RNA probe

Probes for use in microarray experiments were prepared by linear amplification (Liu et al., 2003) but instead of preparing aminoallyl-cDNA probe, aminoallyl-RNA probe was prepared. In brief, DNA obtained by MNase digestion was first treated with calf intestinal phosphatase (New England Biolabs (NEB)) and then thymidine-tailed using terminal dideoxytransferase (NEB). A T7 promoter was adapted to these T-tailed DNA via second strand synthesis with Klenow exo-polymerase (NEB). RNA was next generated using a MegaScript T7 RNA polymerase kit (Ambion) with a 2.3:1 ratio of aminoallyl-UTP to UTP.

Mapping nucleosome positions using tiling microarrays

Nucleosome positions were mapped using a 20bp resolution tiling microarray with the majority of the probes being identical to a previously described microarray version (Yuan et al., 2005). We designed the remaining probes, which included coverage of the *PRM1* ORF. This

tiling microarray was printed using a custom arrayer and consisted of 32 print blocks with a total of 16,429 bona fide probes. Unless otherwise specified, nucleosomes were mapped in four independently grown cultures for each strain by hybridizing 5μg of mononucleosomal-sized probe and 5μg of reference genomic DNA probe. Hybridizations were conducted at 65° C for at least 12 hr prior to scanning. Dye swaps were incorporated into the experiments in a balanced manner such that with four mononucleosome:reference replicates, two were labeled as Cy3:Cy5 and the remaining two Cy5:Cy3.

Microarray data processing

Raw microarray data was processed and analyzed using custom-written software implemented with Python. Algorithms for statistical analysis were provided by the R statistics software package. A mononucleosome:reference ratio was calculated for each feature by first subtracting the feature median background intensity from the feature foreground intensity and then taking the log base 2 transformed ratio. The feature ratios in each print block were normalized for intensity-dependent bias using a LOESS regression algorithm with a smooth value of 0.4 (LOESS function provided by the R statistics package).

Preparing nucleosome position data for analysis

Analysis of nucleosome enrichment data was done using custom-written software implemented with Python that integrated statistical algorithms from the R statistics package. Nucleosome enrichment values for each experiment were determined by taking the mean of the experiment replicates and applying a centered moving average with a window of 5 features (100 bp). This moving average was strictly implemented such that no missing values were permitted within the window, and each feature in the window must be offset by 20 bp (the array resolution) from its immediate neighbor.

Generation of difference maps

While results from two experiments can be compared side-by-side, generation of a difference map that represents differences between experiments is useful to highlight how the datasets differ from one another. As nucleosome enrichment data are in log2 space, difference maps were generated by subtracting probe data for a control experiment from corresponding probe data for the second experiment. For example, to generate the difference map shown in Fig. 3A, probe data from a control experiment that lacked the Reb1 degron were subtracted from corresponding probe data from an experiment that contained the Reb1 degron. The strains used for both experiments were grown under the same conditions.

Analysis of nucleosome position data as a one-dimensional line trace

Nucleosome positioning data shown in the Figures were generated by the Matplotlib plotting engine module for Python using a coordinate system with probe data representing nucleosome positions overlaid on the positions of features in the genome.

Generation of two-dimensional stacks of nucleosome positioning data and alignment of data at the boundary between NFRs and their downstream nucleosomes

Comparison of nucleosome positions among a set of ORFs is easily achievable by generating a two-dimensional stack in which each row represents data associated with one ORF and each column represents probe data that is relative to a defined reference point in each ORF. These two-dimensional stacks were generated using custom-written Python software for graphical visualization with Java TreeView.

For the specific purposes of this work, all two-dimensional stacks were generated for ORFs that were associated with probe data. As the resolution of the tiling microarray platform is

20bp, bins of 20bp were defined relative to the translational start site of each ORF, and available probe data 1000bp upstream and downstream of each ORF were assigned to the appropriate bin by the coordinate representing the last nucleotide of the probe. This process generated a two-dimensional stack of data arranged by ORF, but centered at the translational start site. This is not an ideal arrangement for analyzing nucleosome-free regions as the distance between translational start sites and NFRs can vary among ORFs. Therefore we developed a method of analyzing nucleosome positions about NFRs in a two-dimensional stack of data in which data for each ORF was aligned at the nucleosome downstream of the NFR.

Analyzing experimental data in aligned two-dimensional stacks

Alignments of extracted ORF data at the +1 nucleosome downstream of the NFR were calculated only for experimental data that served as controls. In this work, alignments were calculated using data from a strain isogenic to the degron strains, except that they lacked a degron allele, from a wild-type strain with the Reb1:dT_7 sequence inserted into the *PRM1* gene, and from a *rpb1-1* strain at its permissive temperature. Nucleosome positions for the degron control strain were aligned using data under both degron-inactive and degron-active growth conditions.

Once these alignment maps were generated, experimental data were overlaid onto these maps to determine how nucleosome positioning is affected. For example, nucleosome positioning data from a strain carrying the Sth1-degron grown under degron-inducing conditions were overlaid on the alignment map generated from the control strain grown under the same conditions. Difference maps that highlighted the changes in nucleosome positions between strains were overlaid on alignment maps by first subtracting control probe data from corresponding experimental probe data, and then overlaying the differences onto alignment maps generated from nucleosome positions in the control data.

Acknowledgements

We thank past and present members of our laboratory for discussions and advice over the course of this research. We thank Leslie Chu and Joachim Li for the *pMET3* degron construct. We are especially grateful to Allen Buskirk and David Liu for providing the 4-hydroxytamoxifen-regulated intein construct. This work was supported by a National Institutes of Health Kirschstein predoctoral fellowship (1F31GM083619) to P.D.H. and NIH grant 5R01GM071801 to H.D.M. H.D.M. is a scholar of the Leukemia and Lymphoma Society.

References

Albert I, Mavrich TN, Tomsho LP, Qi J, Zanton SJ, Schuster SC, Pugh BF. Translational and rotational settings of H2A.Z nucleosomes across the Saccharomyces cerevisiae genome. Nature 2007;446:572–576. [PubMed: 17392789]

Angermayr M, Oechsner U, Bandlow W. Reb1p-dependent DNA bending effects nucleosome positioning and constitutive transcription at the yeast profilin promoter. J Biol Chem 2003;278:17918–17926. [PubMed: 12637580]

Barski A, Cuddapah S, Cui K, Roh TY, Schones DE, Wang Z, Wei G, Chepelev I, Zhao K. High-resolution profiling of histone methylations in the human genome. Cell 2007;129:823–837. [PubMed: 17512414]

Beinoraviciute-Kellner R, Lipps G, Krauss G. In vitro selection of DNA binding sites for ABF1 protein from Saccharomyces cerevisiae. FEBS Lett 2005;579:4535–4540. [PubMed: 16083878]

Bernstein BE, Liu CL, Humphrey EL, Perlstein EO, Schreiber SL. Global nucleosome occupancy in yeast. Genome Biol 2004;5:R62. [PubMed: 15345046]

Buskirk AR, Ong YC, Gartner ZJ, Liu DR. Directed evolution of ligand dependence: small-molecule-activated protein splicing. Proc Natl Acad Sci U S A 2004;101:10505–10510. [PubMed: 15247421]

Cairns BR, Lorch Y, Li Y, Zhang M, Lacomis L, Erdjument-Bromage H, Tempst P, Du J, Laurent B, Kornberg RD. RSC, an essential, abundant chromatin-remodeling complex. Cell 1996;87:1249–1260. [PubMed: 8980231]

Cairns BR, Schlichter A, Erdjument-Bromage H, Tempst P, Kornberg RD, Winston F. Two functionally distinct forms of the RSC nucleosome-remodeling complex, containing essential AT hook, BAH, and bromodomains. Mol Cell 1999;4:715–723. [PubMed: 10619019]

De Winde JH, Van Leeuwen HC, Grivell LA. The multifunctional regulatory proteins ABF1 and CPF1 are involved in the formation of a nuclease-hypersensitive region in the promoter of the QCR8 gene. Yeast 1993;9:847–857. [PubMed: 8212892]

Dohmen RJ, Varshavsky A. Heat-inducible degron and the making of conditional mutants. Methods Enzymol 2005;399:799–822. [PubMed: 16338396]

Gavin AC, Bosche M, Krause R, Grandi P, Marzioch M, Bauer A, Schultz J, Rick JM, Michon AM, Cruciat CM, et al. Functional organization of the yeast proteome by systematic analysis of protein complexes. Nature 2002;415:141–147. [PubMed: 11805826]

Guillemette B, Bataille AR, Gevry N, Adam M, Blanchette M, Robert F, Gaudreau L. Variant Histone H2A.Z Is Globally Localized to the Promoters of Inactive Yeast Genes and Regulates Nucleosome Positioning. PLoS Biol 2005;3:e384. [PubMed: 16248679]

Harbison CT, Gordon DB, Lee TI, Rinaldi NJ, Macisaac KD, Danford TW, Hannett NM, Tagne JB, Reynolds DB, Yoo J, et al. Transcriptional regulatory code of a eukaryotic genome. Nature 2004;431:99–104. [PubMed: 15343339]

Ioshikhes IP, Albert I, Zanton SJ, Pugh BF. Nucleosome positions predicted through comparative genomics. Nat Genet 2006;38:1210–1215. [PubMed: 16964265]

Jakobovits EB, Bratosin S, Aloni Y. A nucleosome-free region in SV40 minichromosomes. Nature 1980;285:263–265. [PubMed: 6246449]

Lam FH, Steger DJ, O'Shea EK. Chromatin decouples promoter threshold from dynamic range. Nature 2008;453:246–250. [PubMed: 18418379]

Lee W, Tillo D, Bray N, Morse RH, Davis RW, Hughes TR, Nislow C. A high-resolution atlas of nucleosome occupancy in yeast. Nat Genet 2007;39:1235–1244. [PubMed: 17873876]

Li B, Pattenden SG, Lee D, Gutierrez J, Chen J, Seidel C, Gerton J, Workman JL. Preferential occupancy of histone variant H2AZ at inactive promoters influences local histone modifications and chromatin remodeling. Proc Natl Acad Sci U S A 2005;102:18385–18390. [PubMed: 16344463]

Liaw PC, Brandl CJ. Defining the sequence specificity of the Saccharomyces cerevisiae DNA binding protein REB1p by selecting binding sites from random-sequence oligonucleotides. Yeast 1994;10:771–787. [PubMed: 7975895]

Liu CL, Schreiber SL, Bernstein BE. Development and validation of a T7 based linear amplification for genomic DNA. BMC Genomics 2003;4:19. [PubMed: 12740028]

Lorch Y, Zhang M, Kornberg RD. RSC unravels the nucleosome. Mol Cell 2001;7:89–95. [PubMed: 11172714]

Mavrich TN, Ioshikhes IP, Venters BJ, Jiang C, Tomsho LP, Qi J, Schuster SC, Albert I, Pugh BF. A barrier nucleosome model for statistical positioning of nucleosomes throughout the yeast genome. Genome Res 2008a;18:1073–1083. [PubMed: 18550805]

Mavrich TN, Jiang C, Ioshikhes IP, Li X, Venters BJ, Zanton SJ, Tomsho LP, Qi J, Glaser RL, Schuster SC, et al. Nucleosome organization in the Drosophila genome. Nature 2008b;453:358–362. [PubMed: 18408708]

Meneghini MD, Wu M, Madhani HD. Conserved histone variant H2A.Z protects euchromatin from the ectopic spread of silent heterochromatin. Cell 2003;112:725–736. [PubMed: 12628191]

Nagalashmi U, Wang Z, Waern K, Shou C, Raha D, Gerstein M, Snyder M. The transcriptional landscape of the yeast genome defined by RNA sequencing. Science 2008;320:1344–9. [PubMed: 18451266]

Ng HH, Robert F, Young RA, Struhl K. Genome-wide location and regulated recruitment of the RSC nucleosome-remodeling complex. Genes Dev 2002;16:806–819. [PubMed: 11937489]

Nonet M, Scafe C, Sexton J, Young R. Eucaryotic RNA polymerase conditional mutant that rapidly ceases mRNA synthesis. Mol Cell Biol 1987;7:1602–1611. [PubMed: 3299050]

Ozsolak F, Song JS, Liu XS, Fisher DE. High-throughput mapping of the chromatin structure of human promoters. Nat Biotechnol 2007;25:244–248. [PubMed: 17220878]

Parnell TJ, Huff JT, Cairns BR. RSC regulates nucleosome positioning at Pol II genes and density at Pol III genes. Embo J 2008;27:100–110. [PubMed: 18059476]

Peckham HE, Thurman RE, Fu Y, Stamatoyannopoulos JA, Noble WS, Struhl K, Weng Z. Nucleosome positioning signals in genomic DNA. Genome Res 2007;17:1170–1177. [PubMed: 17620451]

Raisner RM, Hartley PD, Meneghini MD, Bao MZ, Liu CL, Schreiber SL, Rando OJ, Madhani HD. Histone variant H2A.Z marks the 5' ends of both active and inactive genes in euchromatin. Cell 2005;123:233–248. [PubMed: 16239142]

Reed SH, Akiyama M, Stillman B, Friedberg EC. Yeast autonomously replicating sequence binding factor is involved in nucleotide excision repair. Genes Dev 1999;13:3052–3058. [PubMed: 10601031]

Saragosti S, Moyne G, Yaniv M. Absence of nucleosomes in a fraction of SV40 chromatin between the origin of replication and the region coding for the late leader RNA. Cell 1980;20:65–73. [PubMed: 6248237]

Schones DE, Cui K, Cuddapah S, Roh TY, Barski A, Wang Z, Wei G, Zhao K. Dynamic regulation of nucleosome positioning in the human genome. Cell 2008;132:887–898. [PubMed: 18329373]

Segal E, Fondufe-Mittendorf Y, Chen L, Thastrom A, Field Y, Moore IK, Wang JP, Widom J. A genomic code for nucleosome positioning. Nature 2006;442:772–778. [PubMed: 16862119]

Segal MR. Re-cracking the nucleosome positioning code. Stat Appl Genet Mol Biol 2008;7:Article14. [PubMed: 18454729]

Shivaswamy S, Bhinge A, Zhao Y, Jones S, Hirst M, Iyer VR. Dynamic remodeling of individual nucleosomes across a eukaryotic genome in response to transcriptional perturbation. PLoS Biol 2008;6:e65. [PubMed: 18351804]

Whitehouse I, Rando OJ, Delrow J, Tsukiyama T. Chromatin remodelling at promoters suppresses antisense transcription. Nature 2007;450:1031–1035. [PubMed: 18075583]

Whitehouse I, Tsukiyama T. Antagonistic forces that position nucleosomes in vivo. Nat Struct Mol Biol 2006;13:633–640. [PubMed: 16819518]

Yang JG, Madrid TS, Sevastopoulos E, Narlikar GJ. The chromatin-remodeling enzyme ACF is an ATP-dependent DNA length sensor that regulates nucleosome spacing. Nat Struct Mol Biol 2006;13:1078–1083. [PubMed: 17099699]

Yang YH, Dudoit S, Luu P, Lin DM, Peng V, Ngai J, Spped TP. Normalization for cDNA microarray data: a robust composite method addressing single and multiple slide systemic variation. Nucleic Acids Res 2002;30:e15. [PubMed: 11842121]

Yuan GC, Liu JS. Genomic sequence is highly predictive of local nucleosome depletion. PLoS Comput Biol 2008;4:e13. [PubMed: 18225943]

Yuan GC, Liu YJ, Dion MF, Slack MD, Wu LF, Altschuler SJ, Rando OJ. Genome-scale identification of nucleosome positions in S. cerevisiae. Science 2005;309:626–630. [PubMed: 15961632]

Zanton SJ, Pugh BF. Full and partial genome-wide assembly and disassembly of the yeast transcription machinery in response to heat shock. Genes Dev 2006;20:2250–2265. [PubMed: 16912275]

Zhang H, Roberts DN, Cairns BR. Genome-wide dynamics of Htz1, a histone H2A variant that poises repressed/basal promoters for activation through histone loss. Cell 2005;123:219–231. [PubMed: 16239141]

Zilberman D, Coleman-Derr D, Ballinger T, Henikoff S. Histone H2A.Z and DNA methylation are mutually antagonistic chromatin marks. Nature 2008;456:125–129. [PubMed: 18815594]

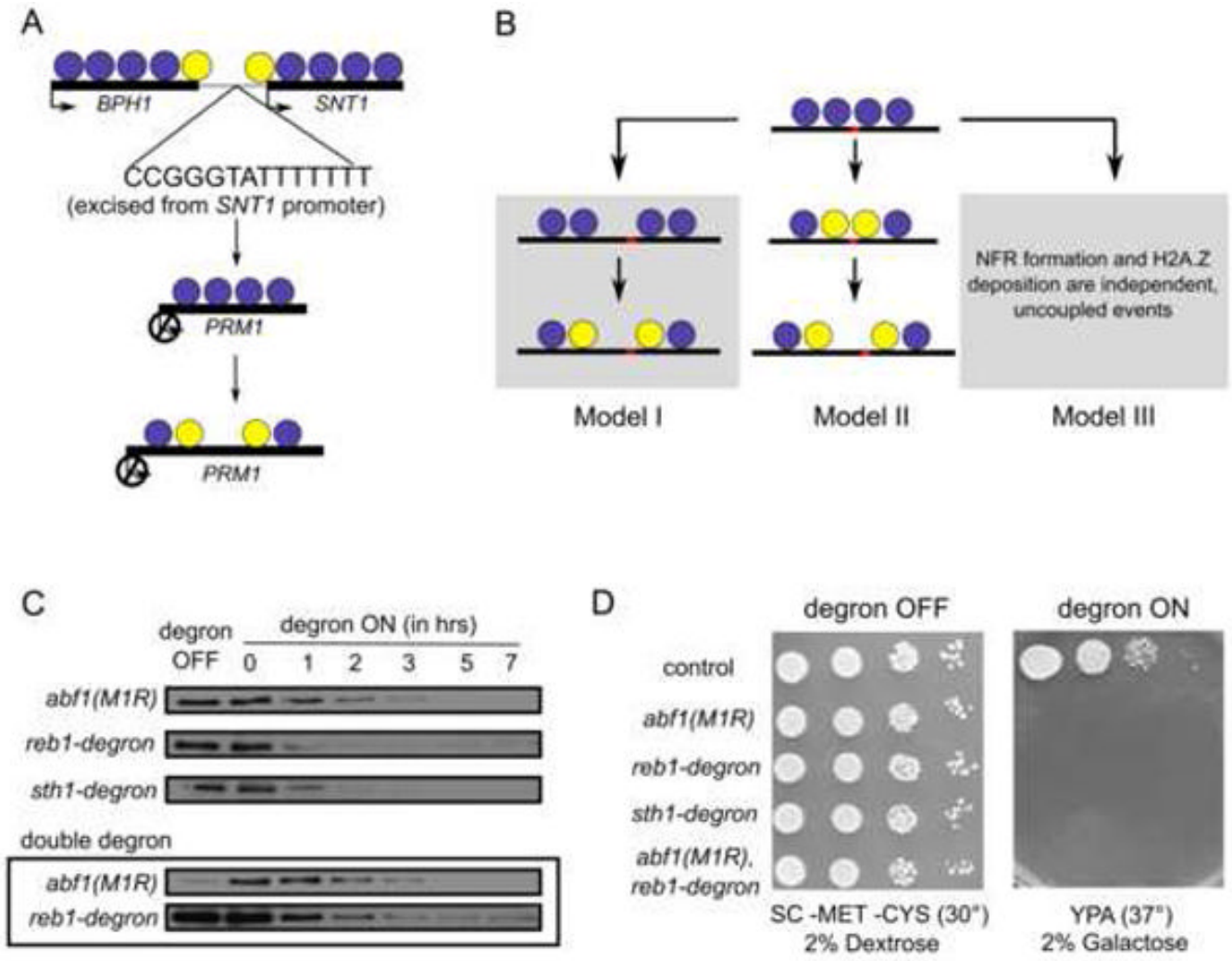

Figure 1. Models and Tools

A. Diagram of the Reb1:dT$_7$ signal used in this study. Circles indicate nucleosomes. Yellow circle indicates H2A.Z variant nucleosome.

B. Models for relationships between NFR formation and H2A.Z deposition

C. Conditional degron alleles of *ABF1*, *REB1* and *STH1* display protein depeletion under degron-inducing conditions. Strains were shifted to YPA media containing 2% galactose for the indicated times and analyzed by immunoblotting with anti-HA or anti-Abf1 antibodies. Ponceau staining of blots demonstrated equal protein loading (Fig. S1)

D. Growth of degron strains under noninducing and inducing conditions. Shown are serial dilutions of strains plated on the indicated media. Plates were photographed after 2 days of incubation.

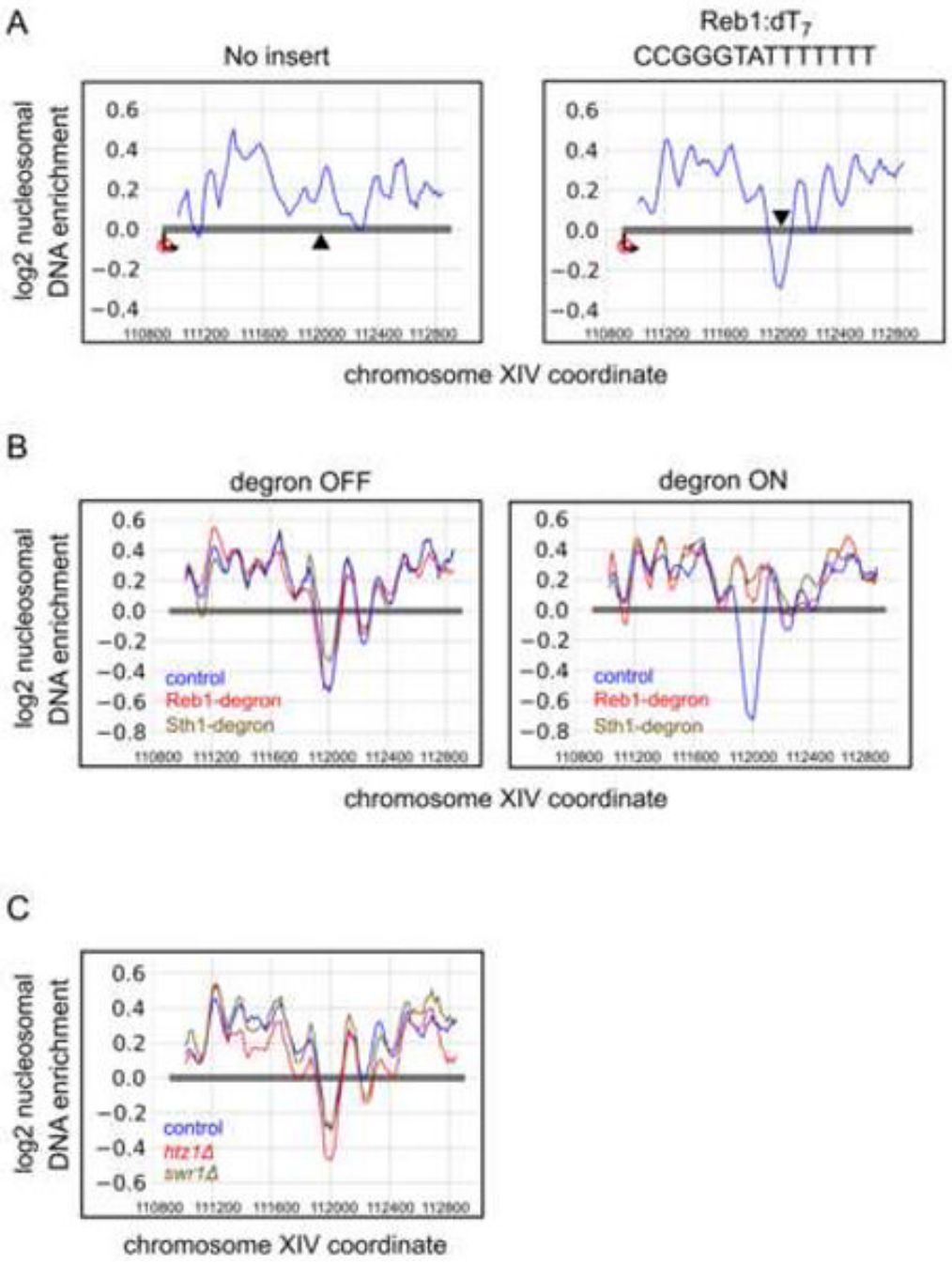

Figure 2. Tiling array analysis of nucleosome positions in the *PRM1* ORF containing the Reb1:dT$_7$ insertion

A. Analysis of the effect of Reb1:dT$_7$ sequence insertion on nucleosome positioning. Shown are line traces of a moving average of mononucleosome/genomic probe signals across the *PRM1* gene with and without the indicated sequence insertion. Triangles indicate the insertion site.

B. Analysis of effects of Reb1 and Sth1 depletion on NFR formation mediated by Reb1:dT$_7$. Indicated strains containing the Reb1:dT$_7$ insertion in the *PRM1* gene were analyzed as described in A.

C. Analysis of effects of *htz1*Δ and *swr1*Δ mutations on NFR formation mediated by Reb1:dT_7. Indicated strains containing the Reb1:dT_7 insertion in the *PRM1* gene were analyzed as described in A.

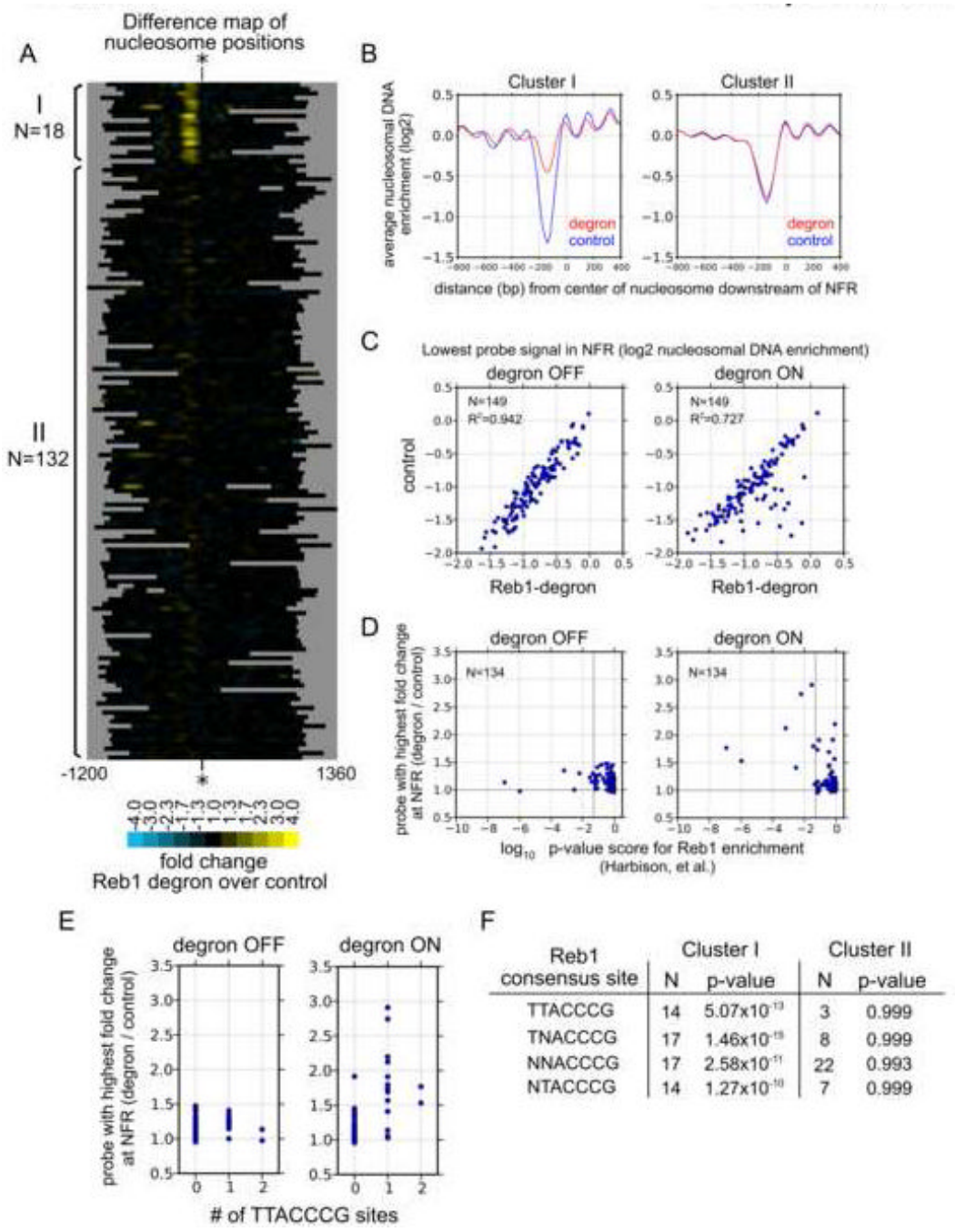

Reb1 consensus site	Cluster I N	Cluster I p-value	Cluster II N	Cluster II p-value
TTACCCG	14	5.07×10^{-13}	3	0.999
TNACCCG	17	1.46×10^{-15}	8	0.999
NNACCCG	17	2.58×10^{-11}	22	0.993
NTACCCG	14	1.27×10^{-10}	7	0.999

Figure 3. Chromosome-wide tiling array analysis of nucleosome positions in cells depleted of Reb1

A. Difference map analysis of effects of Reb1 depletion on nucleosome positions. Map represents nucleosome positioning data from a control strain lacking the Reb1-degron subtracted from a strain with the Reb1-degron. See Experimental Procedures for further details. Nucleosome positioning data 1kb upstream and downstream of the ATG of 150 genes are shown and orientated such that the direction of transcription is to the right. Asterisks indicate center of the +1 nucleosome downstream of the NFR in the control strain. The x-axis represents the distance (in bp) from the center. Data are organized into two clusters using the k-means method.

B. Line traces of average nucleosome positions of the two clusters shown in A The indicated strains were grown under degron-inducing conditions.
C. Scatter plots of the lowest probe signal in NFRs. Points indicate the lowest probe signal in the NFR for a locus in control versus degron strains grown under the indicated conditions.
D. Correlation between Reb1 binding and changes in nucleosomal enrichment at NFRs at promoters. The significance values (log10 p-value) of Reb1 binding at promoters (Harbison, et al. 2004) are compared against the highest fold changes of nucleosome positioning signals at the associated NFR.
E. Correlation between Reb1 consensus sites in promoters and the highest fold change of nucleosome enrichment at the associated NFR under the indicated promoters.
F. Enrichment of Reb1 sites in clusters. Shown are the p-values (hypergeometric testing) of the significance of the indicated Reb1 motifs in the indicated clusters.

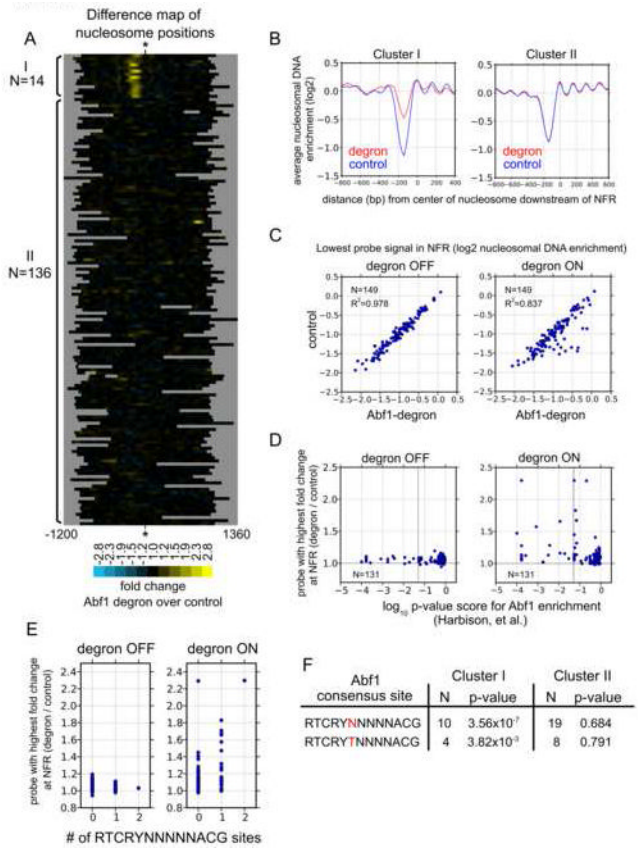

Figure 4. Chromosome-wide tiling array analysis of nucleosome positions in cells depleted of Abf1

A-F. These panels are analogous to those of Figure 3 except that a strain with the Abf1-degron was compared to the same control strain used for analysis of nucleosome positions upon Reb1 depletion.

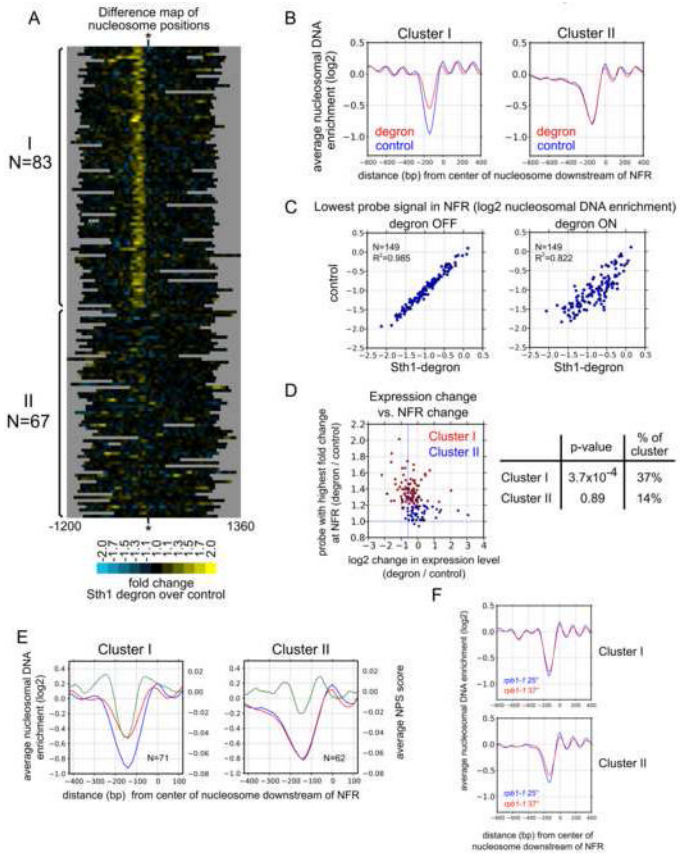

Figure 5. Chromosome-wide tiling array analysis of nucleosome positions in cells depleted of Sth1

A-C. These panels are analogous to those of Figure 3 except that a strain with the Sth1-degron was compared to the same control strain used for analysis of nucleosome positions upon Reb1 depletion.

D. Gene expression analysis. Shown is the correlation between mRNA and NFR changes in cells depleted of Sth1. Ploted are the values for genes on chromosome III. Shown on right is the p-values (hypergeometric testing) of the significance of the enrichments in the indicated gene groups using a 1.5-fold cutoff for decreases in mRNA levels. Expression data were not available for all genes in the clusters; hence, Cluster I N=79, Cluster II N=64.

E. NPS signature averages. Lines traces of NPS predictions (Ioshikes et al., 2006) for genes in the indicated gene clusters are shown in green. These predictions were smoothed using a 51bp moving average window. Experimental nucleosome position averages (control is blue, Sth1-degron is red) are shown as in panel B.

F. Effect of transcription on nucleosome positioning. Shown are the average nucleosome positions for the indicated gene clusters in *rpb1-1* strains grown under permissive conditions or for 1 hr under nonpermissive conditions.

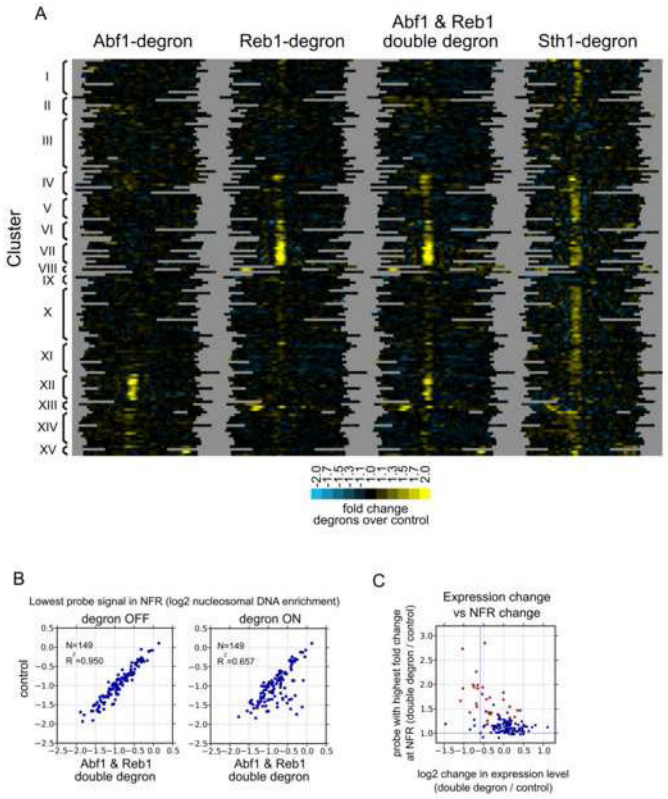

Figure 6. Comparison of the roles of Abf1, Reb1, and RSC in nucleosome positioning

A. Clustering analysis of difference maps. Shown are difference maps for the indicated strains including the Abf1-Reb1 "double degron" strain. K-means (K=15) clustering was applied. Line traces of cluster averages are shown in Fig. S14.

B. Scatter plots of double degron. Analysis was performed as in Fig. 3C.

C. Gene expression analysis. Shown is the correlation between mRNA and NFR changes in cells depleted of both Reb1 and Abf1. The p-value (hypergeometric testing) of the significance of the enrichments in the group of genes (N=20) consisting of those affected in NFR size by Abf1-or Reb1-depletion (Cluster I in Fig. 3 and Cluster I in Fig. 4; corresponding points are colored red in this figure) using a 1.5-fold cutoff for decreases in mRNA levels was 1.2×10^{-6}. The p value for the remaining, unaffected genes (N=123) was 0.99.

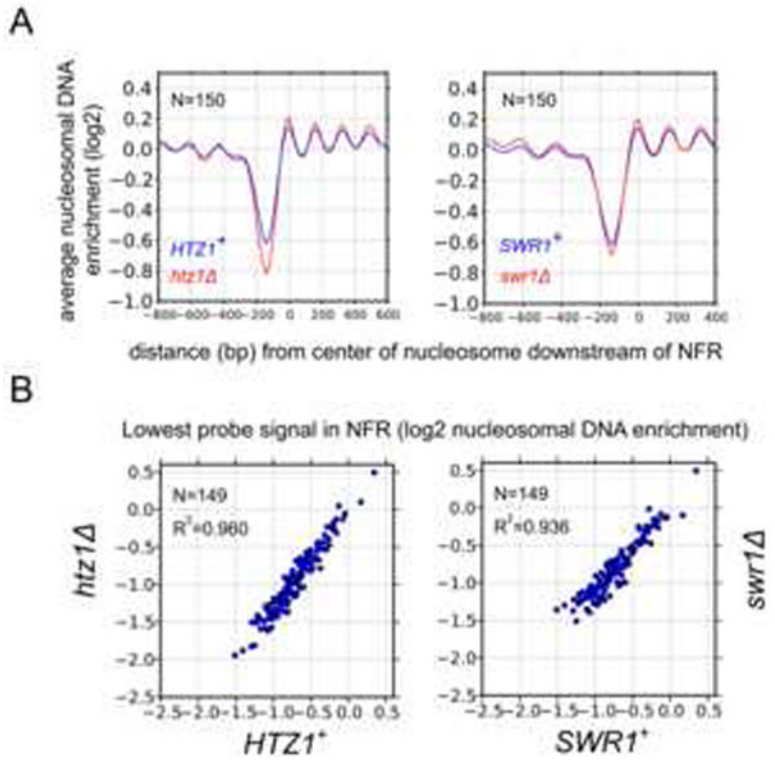

Figure 7. Chromosome-wide tiling array analysis of nucleosome positions in cells defective in H2A.Z nucleosomes

Panels A and B are analogous to Fig. 3B and 3C except that data were derived from cells lacking H2A.Z (*htz1*Δ) or the Swr1 ATPase (*swr1*Δ).

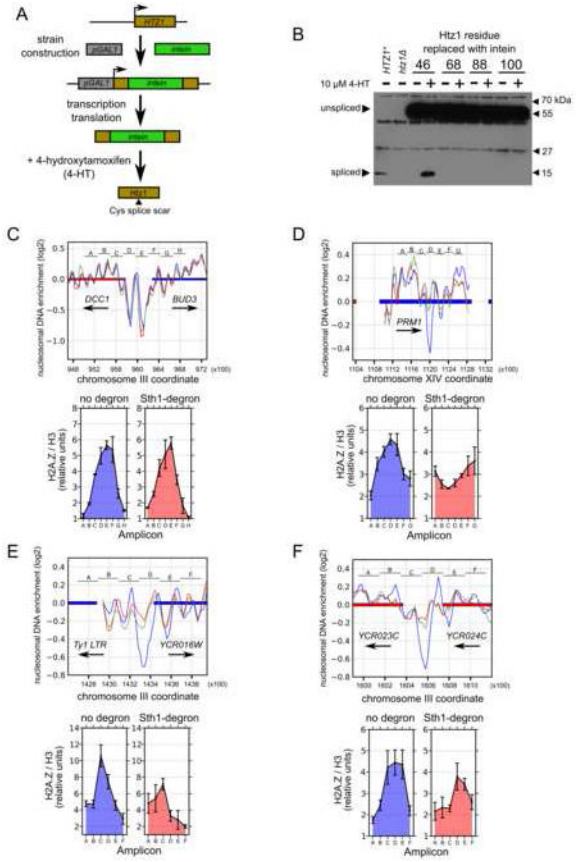

Figure 8. Analysis of H2A.Z deposition requirements using a steroid-regulated intein

A. Schematic of H2A.Z intein constructs. An engineered *M. tuberculosis* RecA intein controlled by the human estrogen receptor ligand binding domain was placed at a chosen site in *HTZ1* gene (encoding H2A.Z). The *HTZ1* promoter was replaced with the galactose-inducible *pGAL1* promoter. Protein splicing would occur in the presence of 4-hydroxytamoxifen (4-HT) and leave a cysteine residue ("scar") at the splicing junction.

B. Splicing of the H2A.Z intein construct occurs with an allele that replaces Ala46 with the intein construct. The 4-HT-regulated intein was inserted in place of four different residues in H2A.Z, and these constructs each were placed on a 2μ plasmid under the control of a *pGAL1* promoter and transformed into a *htz1Δ* strain. Strains were grown to mid-log phase in the presence of 2% galactose and, when indicated, 10 μM 4-HT. Shown is a Western using polyclonal antibody specific to the C-terminus of H2A.Z. A strain with a chromosomal-based, wild-type copy of *HTZ1* and a *htz1Δ* strain are included as controls.

C-F: Analysis of H2A.Z deposition requirements. A strain carrying the Sth1 degron was shifted to degron-inducing conditions which also induces synthesis of unspliced H2A.Z intein construct. After 5 hrs, 4-HT was added to 10μM to induce splicing. Cells were collected after 3 hrs of further incubation, and H2A.Z enrichment at select loci was determined relative to histone H3 enrichment and normalized to a locus in the middle of the large *BUD3* ORF. H2A.Z/H3 enrichment profiles under Sth1-depleted conditions were compared against control profiles. The promoters of *DCC1/BUD3* are analyzed in C; the *PRM1* ORF containing the Reb1:dT_7 insertion is analyzed in D; the promoter of *YCR016W* is analyzed in E, and the promoter of *YCRO23C* is analyzed in F. Top panels of C-F indicate nucleosomal DNA enrichment in various conditions (blue: degron-OFF conditions, red: 5 hrs of degron-ON, green: 8 hrs of degron-ON, with the last 3 hrs in the presence of 4-HT). Bottom panels of C-F represent normalized H2A.Z/H3 enrichment values at the indicated amplicons.